Supplementary Material (2)

Localization errors due to error in model source selection

to

Dipole Characterization Of Single Neurons From Their Extracellular Action Potentials

Ferenc Mechler and Jonathan Victor

Department of Neurology and Neuroscience,
Medical College of Cornell University, New York, NY

Address for correspondence:
Ferenc Mechler
Department of Neurology and Neuroscience
Medical College of Cornell University
1300 York Avenue, New York, NY 10065-4805
phone: (212) 746-6520
Fax: (212) 746-8984
e-mail: fmechler@med.cornell.edu

Summary

Here we consider two related issues. In part A, we determine how the inferred distance to a point source (monopole or dipole) depends on the choice of a source model. This part shows that the idealized analysis of the Discussion – namely, that there is a bias that is proportional to the ratio of the true and assumed exponents (eq.11 in Discussion) of the radial attenuation of the potential – holds when we consider realistic spatial sampling via a multi-contact probe. This analysis also underscores the point that if the assumed exponent is wrong, there can be a large bias in estimating the distance – but this need not be accompanied by a large fitting error.

In part B, we extend this result from point source potentials to a distributed source potential modeled to resemble those generated by a neuronal spike generator. This model source potential had radial symmetry and represented an idealized summary of the radial dependence that we deduced by re-analyzing published data from real neurons or realistic neuron models in Supplementary Material (1). A key feature here is that the dipolar falloff is only valid beyond a minimum distance. We show that once this distance is exceeded, i.e., once within the dipole regime, a dipole model provides both an accurate fit and an accurate localization (it introduces no more than 10%-15% bias towards longer distances). However, at shorter distances than the dipole regime would support, the dipole model fails in a characteristic manner. We identify signature features of this behavior that have diagnostic value, and use them to support results presented in this and a companion paper (Mechler et al. (2011) *Journal of Neurophysiology* doi:10.1152/jn.00515.2010)

To focus on the essential features, all simulations in both parts (A) and (B) assumed an absence of noise and an infinite volume conductor, and ignored the physical properties of the multi-contact probe by reducing it to a set of ideal voltage sampling points in space, one for each contact of the probe. The source-probe separation was uniformly sampled in a spherical volume (between a realistic minimum and maximum distance, 20 μm ≤ d ≤ 200 μm). As in the main text, fitting error was assessed by the fractional mean squared error (MSE), i.e., the MSE divided by the mean squared signal.

Localization error was assessed by ratio of the inferred source-probe distance to the true distance.

The parameters that governed spatial sampling of the potential were not critical to the results. In the model tetrode, contacts were ≈20 μm apart in either square or tetrahedral configuration. To simulate a realistic stepped tetrode experiment, the 4 contacts were rigidly translated in 5, 10, or 20 μm steps over a track of up to 100 μm. We also carried out simulations with an electrode configuration similar to that of a planar silicon polytrode. All these led to qualitatively similar results; we report the simulations of a tetrahedral tetrode advanced in 10 μm steps..

In summary, all simulations assumed

1. infinite volume conductor
2. absence of noise
3. ideal probe with point contacts
4. realistic source-probe separations (i.e., $20 \le d \le 200$ μm)
5. realistic spacing and range of spatial samples (i.e., $10 \le \Delta s \le 100$ μm)

Simulation software was custom written in Matlab. Steps requiring nonlinear optimization were carried out using Matlab's internal *lsqcurvefit* function with Gauss-Newton or trust-region optimization methods.

(A) Low order multipole sources

This set of simulations determines the localization bias that arises due to a mismatch between the 'true' source and a fitted ('model') source. The true source was a monopole, dipole, or a quadrupole plus higher multipolar terms (that result from combining a monopole with a line source; see legend of Figure 1.). The fitted model source was either a monopole, or a dipole. Figure 1 summarizes the results of these simulations.

The most important observation is that there is a systematic and lawful localization bias, as predicted by eq. (11) of the Discussion. In the left two columns, the inferred distance (vertical axis) is shown as a function of the true distance, for monopole fits (column 1), and the dipole fits (column 2). In each case, the points cluster around a line, whose slope is the ratio of the characteristic exponents (k) in the power functions that describe the spatial dependences of the fitted model and the true source. For example, the asymptotic slope equals 1/2 for a monopole fitted to a dipole (middle panel in column 1) and equals 2/3 for a dipole fitted to a quadrupole (bottom panel in column 2). This analytic approximation of the bias is more accurate for the larger number of spatial samples (4-to-8 step experiments) and for the larger distances, and for biases that overestimate rather than underestimate source distance.

The second important observation is that large errors in localization can occur even though goodness-of-fit is high. This is shown in columns 3 and 4, which plot fractional error (vertical axis) against relative localization bias (horizontal axis). Comparably good fits are obtained in simulations in which the correct source model was used (top panel of column 3, middle panel of column 4), or in simulations in which the incorrect source model was used (e.g., middle panel of column 3, or top panel of column 4). The best fits have localization biases that correspond to the estimate of eq. (11), whether or not the bias itself is small. As expected, fit error increases with increasing mismatch in the multipoles (e.g., data clouds from experiments of the same number of steps are shifted upwards from top to bottom panel in column 3), and with the increasing number of spatial samples (as indicated by an upward shift in the data sets that correspond to larger step number in the column 3).

Finally, we mention that one reason that the "wrong" multipole model typically provides a good fit to the data is that the sampling array usually avoids zero-crossings (i.e., does not encounter more than one lobe of the source potential and, in this sense, sampling remains 'local'). The small fraction of simulations that did sample zero-crossings disproportionately contributed to the largest fit errors (fractional MSE>10^{-2}) and exhibited highly unpredictable localization behavior.

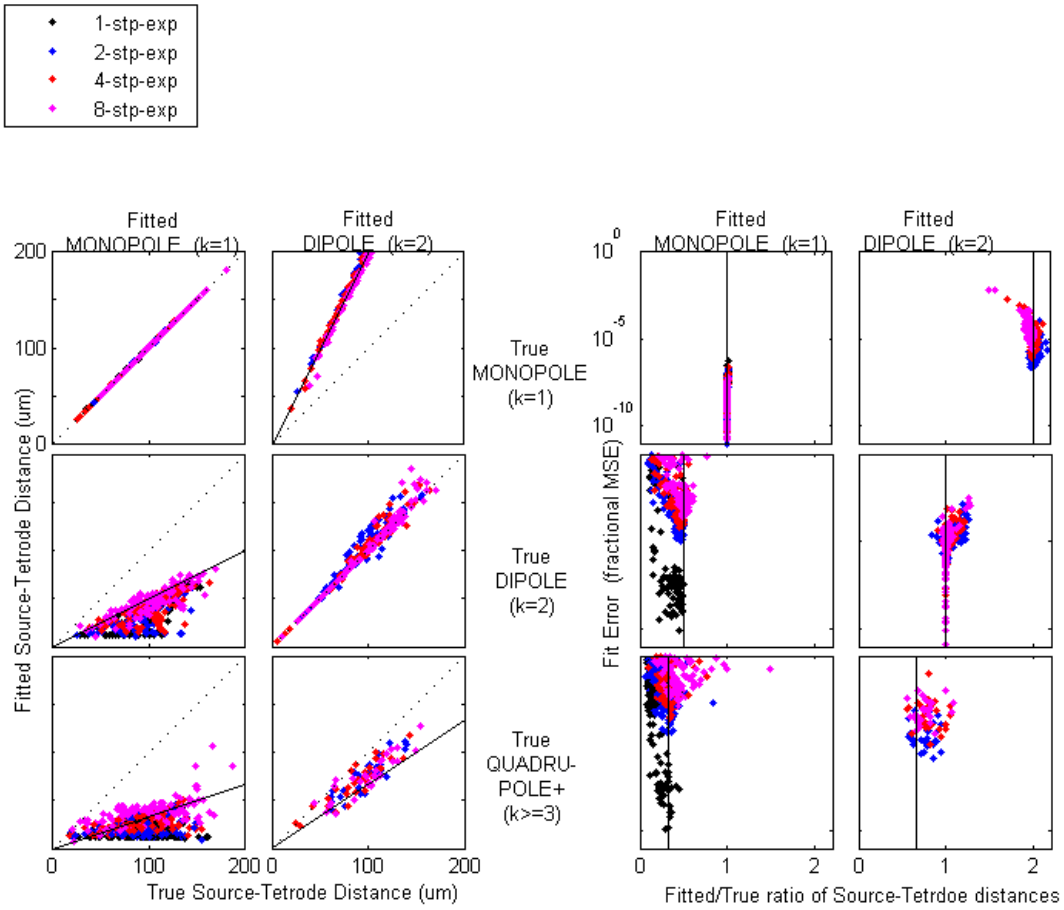

Figure 1

Fitting a model multipole to the potential of a given ("true") multipole source. The potential is spatially sampled in stepped-tetrode experiments (4 experiments, with 1, 2, 4, or 8 steps each). Tetrode contact configuration was a 20-µm-tetrahedron. 100 simulations were run per condition, each with a random cell location. Quadrupole+ is a combination of a negative monopole superimposed at the center on a positive evenly distributed finite line source of equal combined strength. This current distribution has the quadrupole as the first nonzero term in its multipole expansion.

(B) Dipole localization of a distributed source with a realistic EAP decay

In this section, we extend the above analysis to quantify the conditions that support accurate dipole localization of real spiking neurons. Rather than simulate a realistic cable model of neurons, we use a semi-analytic potential function distilled from real spiking neurons or realistic cable models themselves (see our analysis of such published data in Supplementary Material (1)). That analysis leads to the following three features of the potential function, which we build into the simulations: (*i*) the potential function has spherical symmetry; (*ii*) the potential function decreases monotonically with distance from the soma, in a manner that the exponent k of the locally best fitting power function $V(r) \sim r^{-k}$ increases with distance; and (*iii*) there is a critical distance, r_0, where the exponent reaches the value 2 and stops increasing. The regime $r \geq r_0$ is thus the dipole regime: in this range, $k(r) = 2$ and $V(r) \sim r^{-2}$. To implement these features, we use a continuous concatenation of power functions with a constant exponent within each successive interval of r (see top row of Figure 2), and chose 3 values of the lower bound of the dipole regime, $r_0 = \{30, 40, 50\}$. These values are consistent with the numerous data sets that we reanalyzed in Supplementary Material (1)). Other details of the simulations were as in Part A.

Figure 2 summarizes the results of the simulations. The bias in dipole localization (second row of plots, shown as in the leftmost columns in Figure 1) is slight and consists mostly of a modest (≈10-15%) over-estimation of the source-probe separation at most distances (data above the diagonal identity line). Interestingly, intercept and slope parameters extracted by regression analysis indicate that, for larger values of r_0 (representing larger or more distributed current sources), the bias behaves in a more additive (and less multiplicative) fashion. This can also be seen by comparing the histograms of the true and fitted distances (third row): the shift in the mean of the histogram is smaller for larger sources (third column) than small sources (first column), but the depletion of the smallest distances shows the opposite trend.

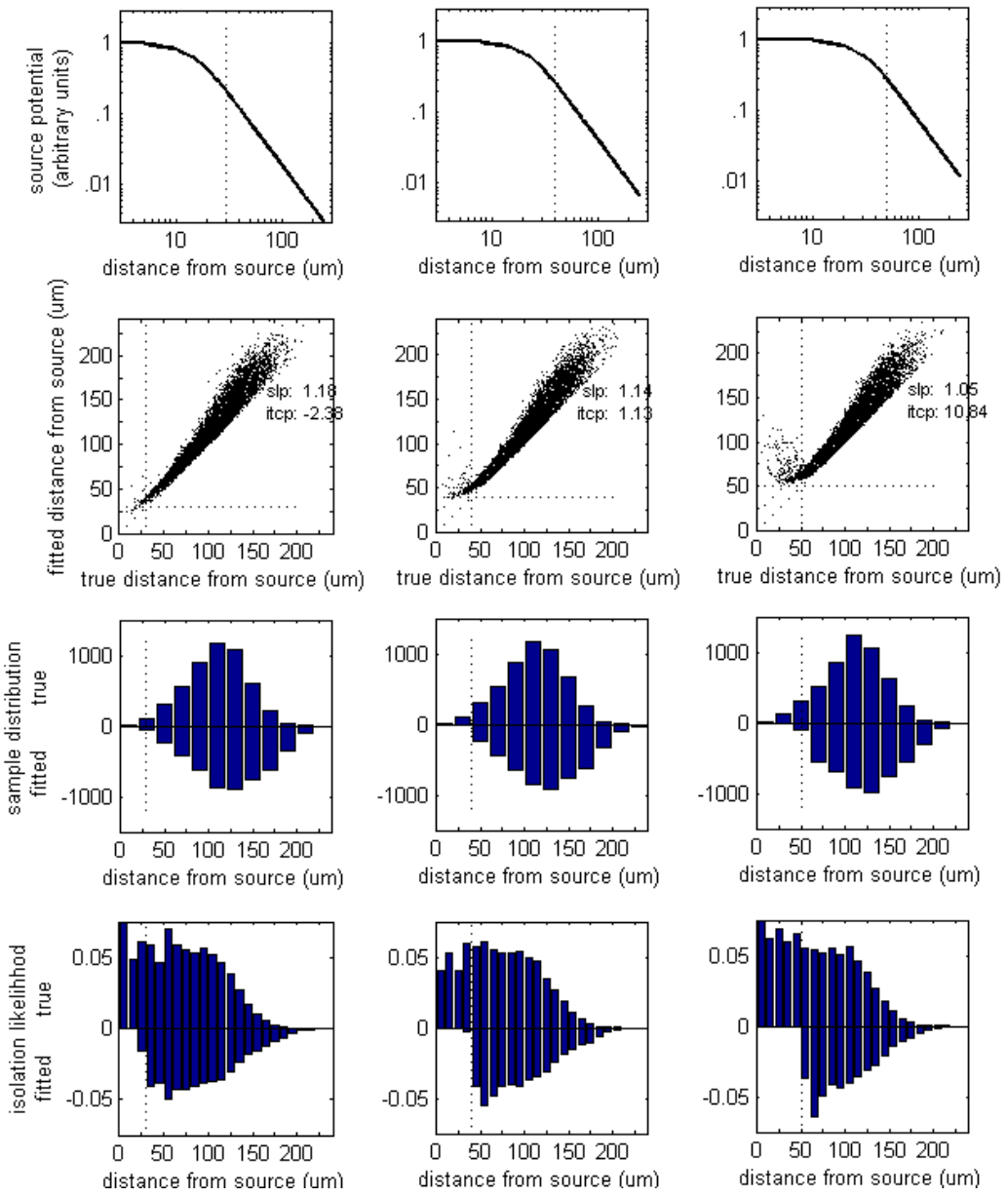

Figure 2

Fitting a model dipole to the potential of a modeled neural source. The radial dependence of the spherically symmetric source potential is plotted in the top row. Vertical lines indicate r_0. Dipole regime holds for $r > r_0$; for $r \le r_0$, the dipole model is a poor approximation of the source potential. Simulated tetrode experiments were all 4-step. Tetrode contact configuration was a 20-µm-tetrahedron. 5000 simulations were run for each condition, each simulation with a random cell location. Second row: scattergram of true and inferred source-probe distances. Third row: histogram of these distances. Fourth row: volume-corrected histogram. In rows 3 and 4, positive and negative valued histograms represented model fits and 'true' data, respectively.

This behavior is diagnostic of the way in which the dipole approximation fails. At $r \le r_0$ (where the dipole model fails), it introduces a severe upward bias in those distance estimates. The failed dipole model maps real source-probe distances in the range $r \le r_0$ to inferred source-probe distances in the range $\tilde{r} > r_0$. As a consequence of the exponent rule discussed above, the smallest true distances (smallest *r*, for which the effective exponent is closest to 1) are subject to the largest biases. Effectively, this mis-estimation of distances corresponds to a mirror placed at r_0 (indicated as a horizontal line in the second row of the plots). Since this behavior affects a larger fraction of the neurons as r_0 increases, we see its effects more prominently in the third column ($r_0 = 50$), than in the first column ($r_0 = 30$).

In sum, we identify two signatures of the short-distance failure of dipole localization of real neurons. These are highlighted in the volume-corrected version of the probability distribution (bottom row of plots), which takes into consideration that uniform sampling of space results in larger number of samples at larger distances. The two features are (i) a systematic under-representation of cells at close encounters (indicated by the reduced isolation likelihood at short distances, as shown by the down-pointing histograms in the bottom row); and (ii) an increased apparent isolation likelihood at $r_0 < r < 2r_0$ distances manifest in a small local likelihood peak $r \sim 70\,\mu\text{m}$. The latter results from the short distances subset that are reflected by the hard lower bound on modeled distances at r_0.